



# Evaluation of welding characteristics using three-dimensional finite element simulation and experimentation for FSW of aluminum 6061

K. Venkata Rao<sup>1</sup>

Received: 18 July 2017 / Accepted: 2 January 2018 / Published online: 29 January 2018  
© The Brazilian Society of Mechanical Sciences and Engineering 2018

## Abstract

Aim of this study is to introduce numerical 3D finite element method (FEM) simulation to study characteristics of friction stir welding. A coupled experimental and numerical simulation study was carried out to study the effect of process parameters on welding characteristics for friction stir welding of aluminium 6061. As per Box–Behnken design, 15 experiments have been conducted on aluminium 6061 plates at three levels of spindle speed, tilt angle and tool pin diameter. Experimental results of tool vibration, force in  $X$ ,  $Y$  and  $Z$  directions and ultimate tensile strength were collected and analyzed. Shearing of metal and metal flow patterns during the welding were analyzed and the responses were predicted using FEM simulation. Size of the shear zone around the tool pin was studied for different combinations of the parameters. The experimental results and the FEM-simulated values were found to be in good agreement. Interaction effect of the process parameters on the responses was analyzed using response surface methodology.

**Keywords** Friction stir welding · FEM simulation · Tool vibration · Welding forces · Shearing of metal

## 1 Introduction

Friction stir welding (FSW) is one type of solid phase welding developed in 1991 at The Welding Institute [1]. The friction stir welding was proved as one of the best metal joining techniques for similar and dissimilar alloys [2]. The schematic diagram of FSW is shown in Fig. 1, where pin of rotating tool is inserted in the plates and moved along the joint. During the process, the tool vibrates in  $X$  and  $Y$  directions. Axial vertical force ( $F_z$ ) applied by the tool and forces exerted in  $X$  ( $F_x$ ) and  $Y$  ( $F_y$ ) directions have significant effect on the weld quality along with the tool vibration. FSW is found to be a suitable method for fabrication of Tailor Welding Blanks which are frequently used in aerospace, automobiles and other applications. The FSW is also useful to weld dissimilar metals. Quality of welds made by FSW is affected by the process parameters.

Hence it is required to study effect of process parameters on the welding quality characteristics and optimize the process parameters [3]. When the rotating welding tool moves along the welding path, material in front of the tool opposes the tool motion. To overcome the material resistance, it is required to apply more force in welding direction ( $Y$  direction) which is called as welding force. The other two forces called as vertical ( $Z$  direction) and lateral ( $X$  direction) forces also considered in the analysis in order to study their influence on the welding. It was concluded that the lateral force has less effect on the FSW [4].

Researchers have been working in the area of FSW to study the welding quality characteristics and optimize process parameters. Some of the researchers are also using finite element methods (FEM) numerical simulation methods to study the effect of the process parameters on the welding quality characteristics. Optimization techniques like response surface methodology (RSM), Taguchi method, grey relation analysis, artificial neural networks, have been used in FSW to optimize process parameters. Morteza et al. [3] used FSW for welding of 6061-T6 aluminum alloy and 5083-H12 thin plates. According to Box–Behnken design, FSW experiments were conducted at different levels of rotational speed, linear speed, shoulder diameter, and tilt angle. Experimental results of tensile

---

Technical Editor: Márcio Bacci da Silva.

---

✉ K. Venkata Rao  
kvenkat\_rama@rediffmail.com

<sup>1</sup> Department of Mechanical Engineering, Vignan's Foundation for Science, Technology and Research, Vadlamudi, Guntur, AP, India

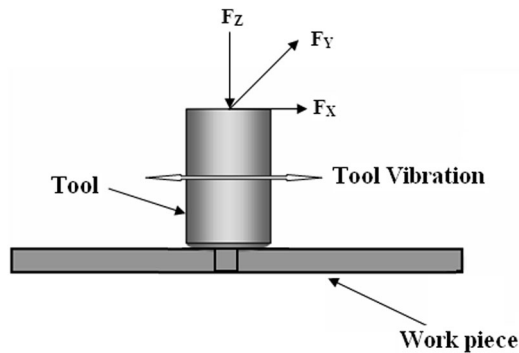


Fig. 1 Schematic diagram of friction stir welding

strength and elongation were analyzed using RSM. The process parameters were optimized for desired responses. Both the optimization and experimental results have good correspondence. Vijay and Adepu [5] studied formation of FSW zone in welding of AA6061-T6 aluminium alloy with macroscopic and microscopic studies. They found good mechanical properties at 1000 rpm of tool speed, welding speed of 40 mm/min and ratio of shoulder-to-pin diameter with value of 3. Buchibabu et al. [6] studied the effect of weld speed, tool rotational speed on welding characteristics for FSW of AA7039 alloy and concluded that the structure, tensile, and impact toughness of the weld were found to be same as the base metal. Sorensen and Stahl [7] studied the effect of tool pin length and diameter on traverse force for welding of AA6061. Pin length has significant effect on the traverse speed, but the pin diameter has less significant effect.

Sxefika and Fatih [8] studied the effect of process parameters like tool rotational speed and feed rate (welding speed) on percentage of elongation, ultimate tensile strength (UTS) and hardness for a welded joint of AA 5083-H111 aluminum alloy. In their work, welding tool with a triangular pin was used. Based on the experimental results, it was observed that the UTS and percentage of elongation of the welded joint were found to be decreased with increase of tool rotational speed. Srinivasan and Manas [9] studied the effect of FSW parameters on mechanical properties of AA2219-T87 welds. As per full factorial experimental design, experiments were conducted at different levels of welding speeds, tool rotational speeds, shoulder diameters and pin diameters at given axial speed. Experimental results of UTS and percentage of elongation of welds were taken for analysis. RSM was used to study interaction effect of process parameters on the responses. Analysis of variance was also used to identify significant parameters. The UTS and percentage of elongation of weld were found to be increased with increase of axial force. The UTS also increases with increase of weld speed and

tool rotational speed. The process parameters were optimized using multi-response optimization.

In FSW, the heat which is generated by the shoulder is more than the heat generated by the probe due to more relative surface velocity of shoulder. Then the heat energy is transformed in the workpiece through the deformation zone. Down force of the tool results generation of heat at shoulder and it increases power consumption [10]. In FSW, material around the tool pin is subjected to plastic deformation and it will become difficult to measure forces due to continuous rotation and translation of tool. To overcome the difficulties, Bipul et al. [11] have designed and developed a measurement system using strain gauge to acquire force signals. They conducted experiments on constant metal and experimental results of force, torque, UTS and yield strength are collected for analysis. They developed support vector regression models to predict the responses for real monitoring. Some authors have reported on use of the ultrasonic vibration in FSW and its influence on the welding characteristics. Zhong et al. [12] introduced the ultrasonic vibration in welding of dissimilar metals like AA6061-T6 to AA2024-T3 and experimental results of traverse force, tool torque and axial force of welding were collected and analyzed. It was concluded that the traverse force, tool torque and axial force were found to be reduced with the use of ultrasonic vibration in FSW.

Friction stir welding phenomena include non-linear deformations, changes in material properties due to welding temperature and shear deformations. That is why researchers have been using numerical simulation methods to study the welding characteristics and effect of the process on welding characteristics [13]. Hamed et al. [13] have studied flow of metal during FSW of copper plates. They used DEFORM-3D to develop numerical simulation models. Material flow patterns, mechanical and metallurgical properties were studied and concluded that the material in front of the tool pin settles at rear side of the tool. Mohammad et al. [14] used FEM approach to study the effect of tool geometry on welding characteristics like force, flow of metal and heat-affected zone in welding of AA5083 aluminum alloy. They conducted experiments at different levels of pin shoulder diameters and results were collected. Artificial neural network models were also developed to correlate the results with FEM and experimental results. Optimum process parameters were identified using these methods. Trimble et al. [15] have developed FEM models to study and predict temperature and tool forces. The predicted values were correlated with the experimental results. The FEM models were used to optimize pin size to improve efficiency of the welding.

Based on the above literature, it was observed that less work was done on the tool vibration during the welding and effect of tilt angle on the welding characteristics. In the

present study, effect of tool rotational speed, pin diameter and tilt angle was studied on the tool vibration, UTS and welding forces in the *X*, *Y* and *Z* directions. A numerical simulation model was developed using DEFORM 3D to study and predict the welding characteristics.

## 2 Workpiece and tool

In the present study, FSW experimental work was carried out on the aluminum 6061 alloy with molybdenum-based high-speed steel tool. It is a precipitation-hardened aluminum alloy and widely used in many industrial applications like aircraft fitting, electrical fitting, couplings, brake pistons, valves and valve parts, camera lens mounts, etc., due to its good mechanical properties and weldability. Chemical composition and mechanical properties of the workpiece metal are given in Tables 1 and 2, respectively. Molybdenum-based high-speed steel has good mechanical properties and its chemical composition is given in Table 3. When the molybdenum is added to high-speed steel beyond 5%, its hardness, toughness and wear resistance are increased.

## 3 Experimentation

Experimental plan was prepared according to Box–Behnken design using welding parameters such as tool rotational speed, tool pin diameter and tilt angle. The experimental plan and results are shown in Table 4. In the present study, the rotational speed, tool pin diameter and tilt angle were selected based on the literature. Sanjay and Sudhir [16] have studied effect of process parameters on performance characteristics and optimized them in FSW of aluminum dissimilar alloys. They conducted experiments beyond the 2000 rpm and tilt angle up to 5°. Another study done by Hossein et al. [17] at pin diameter of 6 mm in FSW of aluminum 6061 alloy. Sato et al. [18] also carried out experiments with spindle rotational speed up to 4000 rpm to study temperature distribution and hardness in FSW. In the present study, tilt angle was taken up to 10°, that is why the tool rotational speed was taken up to 3000 rpm.

As shown in Fig. 2, experiments were conducted on aluminum 6061 alloy with molybdenum-based high-speed steel tool on CNC vertical machining center. The tool has 12 mm shoulder diameter. A PolyTech 100-V laser Doppler vibrometer (LDV) was placed in front of the machine

and the laser beam is focused on the tool to measure its vibration. The LDV is a non-contact type sensor that produces a laser beam towards rotating object (tool) to measure its vibration in terms of acousto optic emission signals. A fast Fourier transformer was used to process the acousto optic emission signals and convert them into frequency domain to read the amplitude of the cutter vibration directly as shown in Fig. 3. KISTLER 9257B type dynamometer is a platform-type piezoelectric force dynamometer used in the present study to measure forces induced in *X*, *Y* and *Z* directions. The dynamometer consists of three force-sensing components to measure the forces in three directions and there is a digital display connected to the three components of the dynamometer. Simultaneous measurement of the forces in the three directions during the welding helps to understand the FSW mechanism and optimize process parameters [19]. As shown in Fig. 2, the dynamometer is rigidly held on the table and the work locating device was also rigidly fixed on the dynamometer. During the FSW process, the forces are directly recorded from the dynamometer display. After completion of the experiments, UTS was measured on computerized universal testing machine. Welded joints of six different experiments are shown in Fig. 4.

## 4 FEM simulation

In the present study, DEFORM-F23 version 10.2 was used for numerical simulation of FSW using process parameters which are given in Table 4. The proposed FEM software is capable of simulating welding characteristics like tool vibration, welding forces and shear zones. As shown in Fig. 5, the tool is modeled in CATIA and imported to DEFORM software, where as the workpiece is directly created in the DEFORM software itself. In the simulation, the workpiece and tool were assumed to be rigid-viscoplastic and rigid, respectively. Friction factor and thermal characteristics of workpiece and tool were assumed to be constant [20–22]. Use of traditional Lagrangian-based FEM in FSW simulation leads to distortion of elements due to deformation and convergence issues. Researchers have been developed several techniques to overcome these difficulties and the arbitrary Lagrangian–Eulerian was found to be one among the techniques which has successfully overcome the difficulties [23]. A finite element mesh should consist of linear tetrahedral elements around 50,000 and nodes of 12,500 in order to solve global-level analysis

**Table 1** Chemical composition of Al 6061 metal

Elements	Al	Mg	Si	Cr	Mn	Ti	Cu	Zn	Fe	Others
%	97.30	0.85	0.65	0.15	0.10	0.10	0.20	0.20	0.35	0.10

**Table 2** Mechanical properties of Al 60601 metal

Hardness	UTS (MPa)	% of elongation	Modulus of elasticity (GPa)	Poisson's ratio
95 BHN	310	17	68.9	0.33

**Table 3** Chemical composition of tool metal

Elements	C	Mn	Si	P	S	Ni	Cr	Mo	Cu	Fe
%	1.0	0.33	0.30	0.03	0.008	0.16	3.90	5.20	0.14	balance

**Table 4** Experimental results of responses

Exp. no.	S S (rpm)	Pin dia (mm)	Tilt Angle (°)	Vib. (mm)		UTS (MPa)	$F_X$ (kN)		$F_Y$ (kN)		$F_Z$ (kN)	
				Exp.	Sim.		Exp.	Sim.	Exp.	Sim.	Exp.	Sim.
1	3000	4	5	0.092	0.124	165.4	18.2	27.5	22.9	26.2	16.3	18.2
2	2000	4	5	0.097	0.108	176.9	16.4	15.3	22.1	17.3	17.5	15.4
3	3000	6	5	0.074	0.069	163.1	11.2	12.9	19.8	19.9	15.8	15.9
4	2500	5	5	0.062	0.077	171.7	16.5	18.3	21.0	19.7	13.6	12.5
5	2500	6	0	0.081	0.075	168.5	14.7	15.9	22.8	22.9	16.1	18.2
6	2000	6	5	0.086	0.093	181.9	12.0	12.8	26.0	25.1	18.9	17.0
7	2000	5	10	0.089	0.106	178.3	13.1	12.2	23.7	26.9	13.4	13.1
8	2500	5	5	0.068	0.071	174.0	12.7	12.5	21.0	18.1	16.0	15.6
9	3000	5	0	0.064	0.059	167.2	13.8	14.9	18.1	16.3	14.8	14.2
10	3000	5	10	0.093	0.101	162.8	13.2	12.0	18.7	15.4	15.7	14.5
11	2500	5	0	0.068	0.061	170.7	12.9	13.5	20.0	19.1	13.9	12.4
12	2500	4	10	0.091	0.090	166.7	15.2	16.7	19.9	21.0	15.1	16.5
13	2500	6	10	0.108	0.098	167.0	14.7	15.6	22.8	23.9	16.9	16.6
14	2000	5	0	0.106	0.103	186.2	16.3	18.2	23.3	23.8	15.2	15.5
15	2500	4	0	0.101	0.097	177.8	15.8	16.3	19.2	21.7	15.3	16.7

**Fig. 2** Experimental setup for friction stir welding

[24]. In the present study, the numerical simulation was carried out using arbitrary Lagrangian–Eulerian (ALE) formulation. The workpiece was meshed 60,000 and 13,250 tetrahedral elements and nodes, respectively. Bottom surface and four sides of the workpiece were fully constrained in X, Y and Z directions. The FEM simulation was carried out for the 15 experiments and the responses are predicted and presented in Table 4.

## 5 Results and discussion

As per experimental plan shown in Table 4, experiments were conducted and results were also presented in the same table. Average percentage of deviation between experimental and simulated values was calculated for the amplitude of tool vibration,  $F_X$ ,  $F_Y$  and  $F_Z$  as 6.07, 7.41, 1.52 and 1.98, respectively.



**Fig. 3** Amplitude of tool vibration in frequency domain

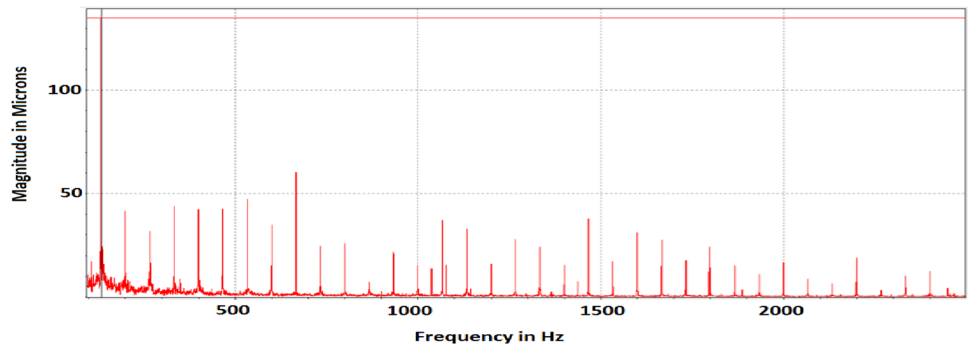


**Fig. 4** Some of the joints produced by FSW

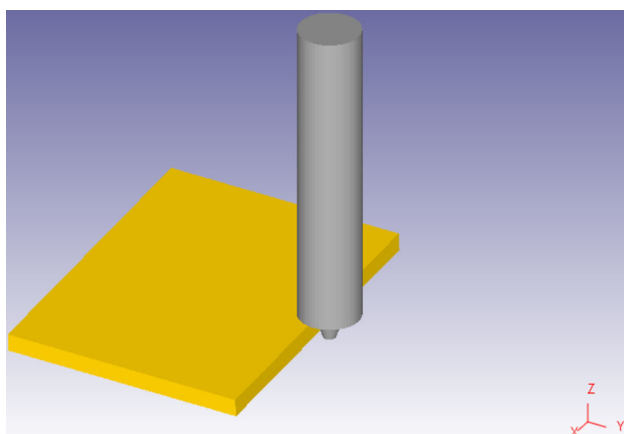
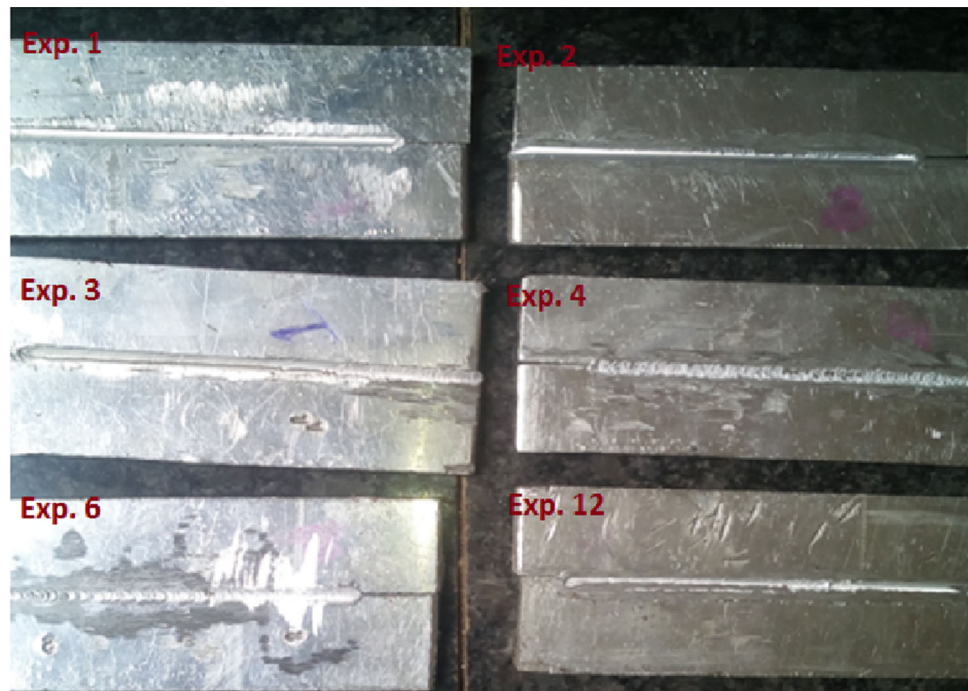


**Fig. 5** Schematic diagram of workpiece and tool

### 5.1 Effect of parameters on the shear deformation

Numerical simulation was also carried out to study the shear deformation of workpiece material for all the experiments. Material around the tool gets sheared and velocity discontinuity is shown in Fig. 6 as boundaries or zones. Metal flow patterns/shear deformation zones are shown in Fig. 6 for randomly selected four experiments. As the rotary tool moves along the weld path, material in front of the tool tends to move back side of the tool and settles there [13, 25]. Stirring action of tool results in generation of frictional heat between bottom surface of the shoulder and top surface of the workpiece. Hence, viscous heat generates in the shear zone. Coefficient of friction and shear deformation of workpiece material affects the heat generation at the stir zone [9]. The shear zone is affected by frictional heat and this zone was considered to be heat-

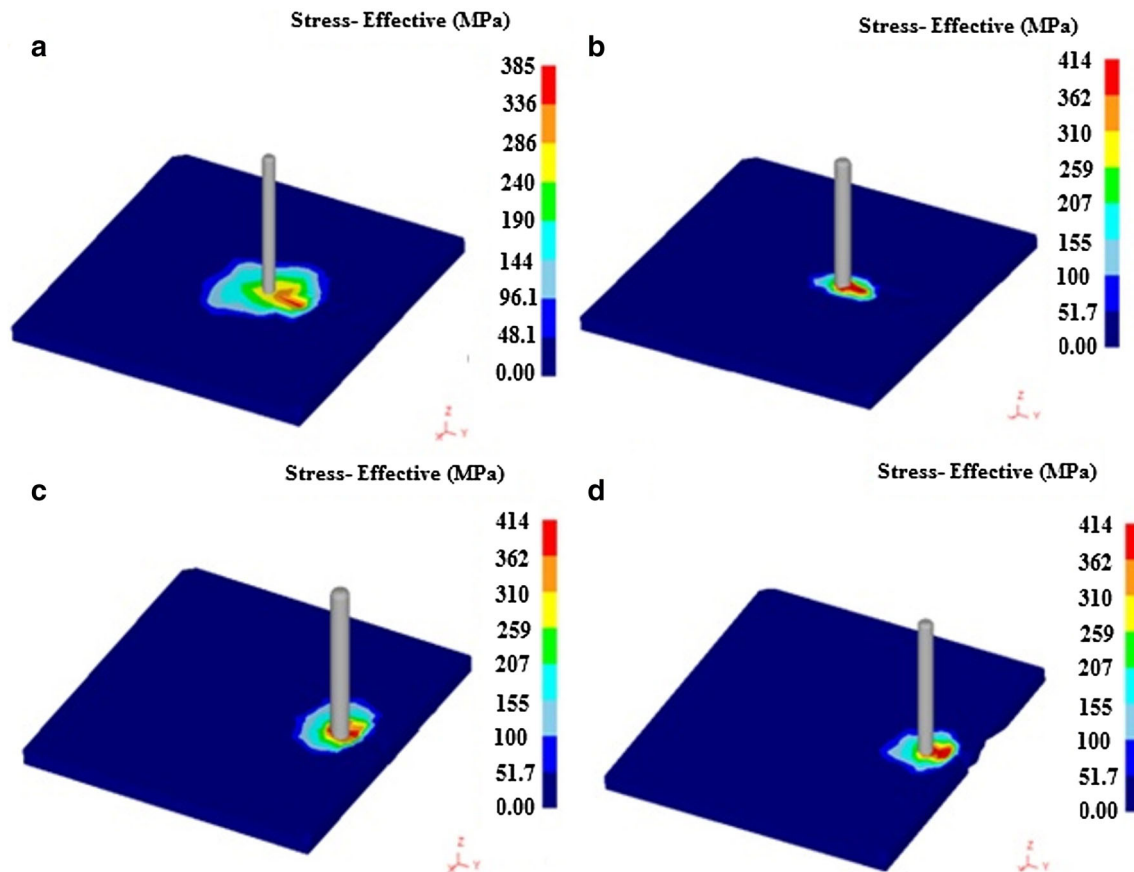


**Fig. 6** **a** Shear zone for Exp. 3; **b** shear zone for Exp. 4; **c** shear zone for Exp. 6 and **d** shear zone for Exp. 12

affected zone. Hence, the heat-affected zone results in fracture at joint and poor weld quality. Mahoney et al. [26] described expansion of heat-affected zone as shoulder diameter is directly proportional to frictional heat. In the present study, tool shoulder diameter was selected as 12 mm and size of the shear zone was studied for 15 experiments.

Shear zone for the Experiments 3, 4, 6 and 12 are shown in Fig. 6. Figure 6a shows a shear zone at 3000 rpm, 6 mm diameter of pin and tilt angle of  $5^\circ$ . Size of the shear zone in this case was found to be high. Figure 6b shows a shear zone at 2500 rpm, 5 mm diameter of pin and tilt angle of  $5^\circ$ . In this case, size of the shear zone was found to be less. Figure 6c shows a shear zone at 2000 rpm, 6 mm diameter of pin and tilt angle of  $5^\circ$ . Figure 6d shows a shear zone at 2500 rpm, 6 mm diameter of pin and tilt angle of  $5^\circ$ . Size of the shear zone in Fig. 6c, d was found to be less than in Fig. 6a and more than in Fig. 6c, d. It was observed that the size of shear zone is affected by tool rotational speed and diameters of pin. But the tilt angle does not have a significant effect.

## 5.2 Effect of process parameters on tool vibration

Numerical simulation of the tool vibration was carried out for all the experiments and presented in Table 4. Closeness was observed between the simulated results and experimental results of tool vibration for all the experiments. Figure 7 displays the simulated tool vibration of one such case where the tool rotational speed is 3000 rpm, pin diameter and tilt angle are 4 mm and  $5^\circ$ , respectively.

Interaction effect of process parameters on the tool vibration for all the 15 experiments carried out in the present study is shown in Fig. 8. Effect of tool pin diameter at different speeds on the tool vibration is shown in Fig. 8a. The amplitude of tool vibration reduces when the spindle speed is increased for 4 mm diameter of pin, while it has increased with an increase in the spindle speed for a pin diameter of 6 mm. The vibration amplitude is practically unaffected with increase in spindle speed for the case of 5-mm-diameter pin. However, this increase continues up to a spindle rotational speed of 2600 rpm and subsequently

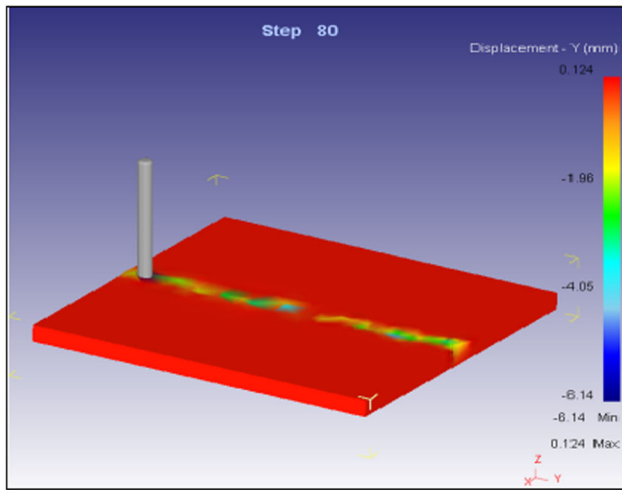


Fig. 7 Simulated tool vib. for the Exp. 1

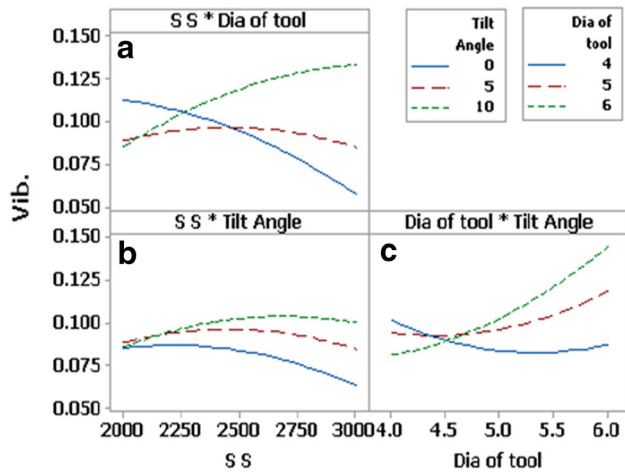


Fig. 8 Interaction effect of parameters on tool vib

displays a trend of reduction. A similar trend has been observed for tilt angle, where the increase in amplitude of vibration was found till a speed of 2500 rpm and thereafter, it decreases. For the case of 0° tilt angle, a monotonic decrease in the vibration was recorded.

Effect of tilt angle at different speeds on the tool vibration is shown in Fig. 8b. There is a slight increase in the amplitude of tool vibration, as the spindle speed increases for a tilt angle of 10°. However, tool vibration amplitude reduces for a tilt angle of 0°. Figure 8c depicts the effect of tilt angle at different pin diameters on the tool vibration. Amplitude of tool vibration increased for tilt angles 5° and 10° when the pin diameter is increased, whereas the vibration amplitude was found to be reduced as the pin diameter is increased. The amplitude of vibration has shown an increasing trend for both 5° and 10° tilt angles, while the contrary trend was observed for the 0° tilt

angle. Further, a relative increase in the amplitude of vibration for 10° in comparison with 5° was noted.

### 5.3 Effect of process parameters on $F_X$

Numerical simulation for the tool force in X direction was carried out for all the experiments and presented in Table 4. Closeness was observed between the simulated results and experimental results of  $F_X$  for all the experiments. Figure 9 displays the simulated results of  $F_X$  of one such case where the tool rotational speed is 3000 rpm, pin diameter and tilt angle are 4 mm and 5°, respectively.

Interaction effect of process parameters on the  $F_X$  for all the 16 experiments carried out in the present study is shown in Fig. 10. Effect of tool pin diameter at different speeds on the tool vibration is shown in Fig. 10a. The  $F_X$  was found to be high for tool pin diameter of 4 mm and it slightly increases from 2000 to 3000 rpm of tool rotational speed. The  $F_X$  shows reduced trend from 4 to 6 mm diameter of tool pin. But, there is significant reduction in  $F_X$  for tool pin diameter of 6 mm from 2000 to 3000 rpm of tool rotational speed.

Interaction effect of tilt angle and spindle rotational speed on the  $F_X$  is shown in Fig. 10b. There is no significant change in  $F_X$  for tilt angle of 10°, the tilt angle of 5° has slight reduction in the  $F_X$  from 2000 to 3000 rpm of tool rotational speed and the  $F_X$  reduces from 2000 to 3000 rpm of tool rotational speed for the tilt angle 0°. Interaction effect of tilt angle and diameter of tool pin on the  $F_X$  is shown in Fig. 10c. The  $F_X$  shows reduced trend for the three tilt angles from 4 to 6 mm diameter of tool pin. There is sharp reduction in the  $F_X$  for the tilt angles 0° and 5°.

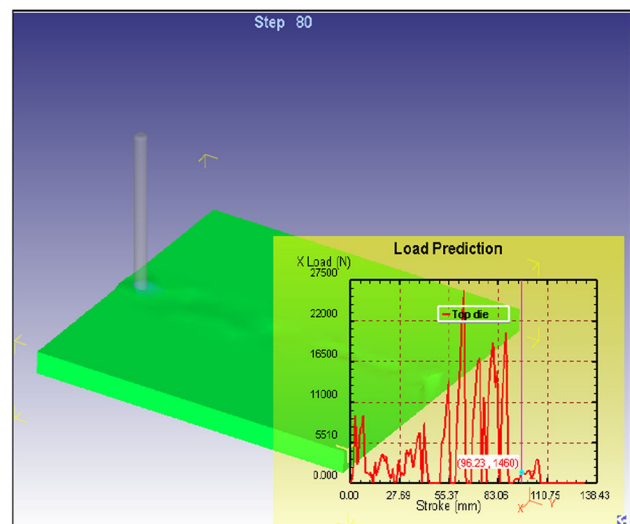


Fig. 9 Simulated result of  $F_X$  for the Exp. 1

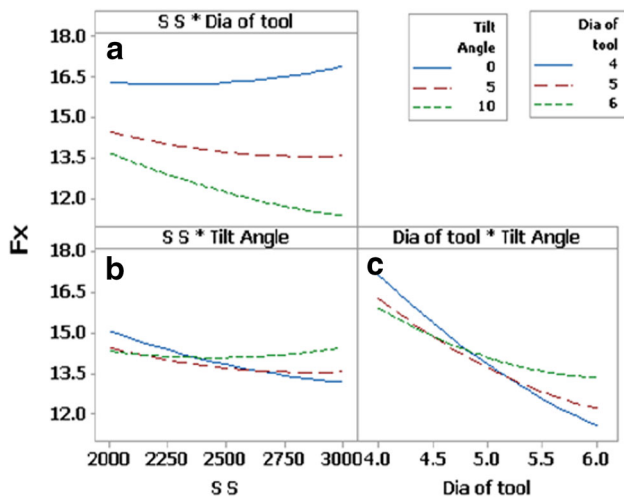


Fig. 10 Interaction effect of parameters on  $F_x$

### 5.4 Effect of process parameters on $F_Y$

Numerical simulation for the tool force in Y direction was carried out for all the experiments and presented in Table 4. Closeness was observed between the simulated results and experimental results of  $F_Y$  for all the experiments. Figure 11 displays the simulated results of  $F_Y$  of one such case where the tool rotational speed is 3000 rpm, pin diameter and tilt angle are 4 mm and  $5^\circ$ , respectively.

From Fig. 12a, it can be observed that, for irrespective values of the tool diameters and tilt angles, 4 mm diameter of tool pin, increase in the spindle speed from 2000 to 2500 rpm caused a decrease in  $F_Y$ , while further increase in spindle speed to 3000 rpm caused a rise the  $F_Y$ . Also at 3000 rpm, both 5 and 6 mm tool pin diameters cause same level of welding force  $F_Y$ . In Fig. 10, the effect of the

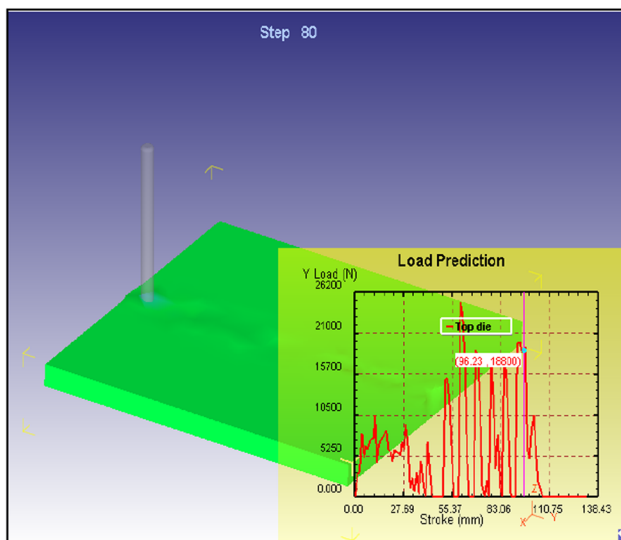


Fig. 11 Simulated result of  $F_Y$  for the Exp. 1

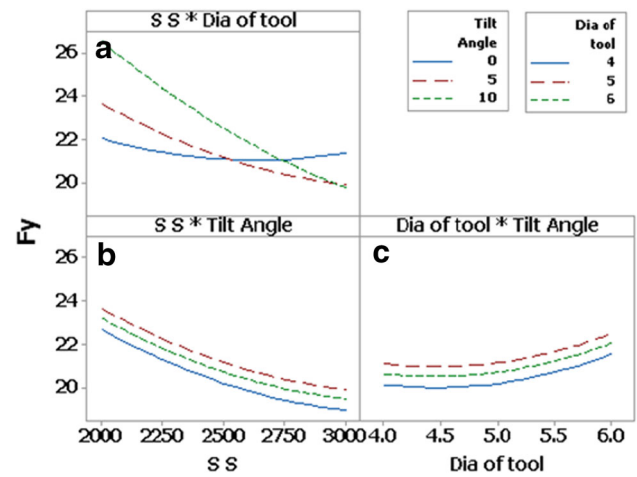


Fig. 12 Interaction effect of parameters on  $F_Y$

process parameters, spindle speed, tilt angle and tool pin diameters on the  $F_Y$  is shown. Figure 12b shows the variation of  $F_Y$  with respect to the tilt angle at various levels of spindle speed. It was observed that, tilt angle  $0^\circ$ , i.e., an upright vertical tool gives the minimum welding force in Y direction at higher levels of the spindle speeds from 2500 to 3000 rpm. With increase in the tilt angle to  $5^\circ$ , a rise in the  $F_Y$  was noted. Further increase in the tilt angle to  $10^\circ$  also records a rise in the force.

In Fig. 12c, the effect of tilt angle at the three different diameters was shown. Irrespective of the tilt angle considered in the present study, the increase in the tool diameter from 4 to 5 mm caused a very slight reduction in the value of  $F_Y$ . However, further increase of tool pin diameter from 5 to 6 mm caused increase in the  $F_Y$  from 21 to 23.5 kN.

### 5.5 Effect of process parameters on $F_Z$

Numerical simulation for the tool force in Z direction was carried out for all the experiments and presented in Table 4. Closeness was observed between the simulated results and experimental results of  $F_Z$  for all the experiments. Figure 13 displays the simulated results of  $F_Z$  of one such case where the tool rotational speed is 3000 rpm, pin diameter and tilt angle are 4 mm and  $5^\circ$ , respectively.

The effect of parameters on the vertical force  $F_Z$  is shown in Fig. 14. In Fig. 14a, b, the dependency of  $F_Z$  on the tool pin diameter and tilt angle at 2000, 2500 and 3000 rpm of spindle speeds are shown, respectively. It was observed from Fig. 14a that with increase in the spindle speed, both the 4- and 5-mm diameters of tool pin caused an increase in the  $F_Z$ , while the opposite happened for the 6-mm tool pin diameter. Also a relative sharp rise in the  $F_Z$  for 4 mm tool pin diameter was noted from 2000 to 3000 rpm of spindle speeds.



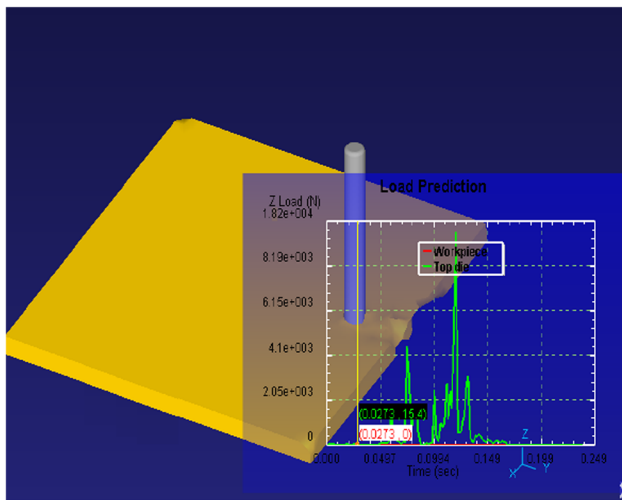


Fig. 13 Simulated result of  $F_z$  for the Exp. 1

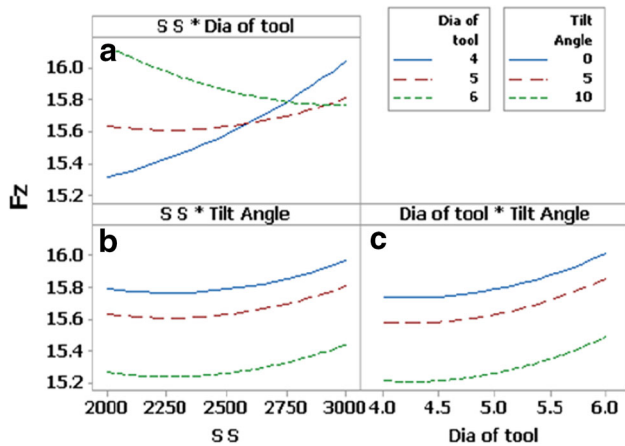


Fig. 14 Interaction effect of parameters on  $F_z$

Figure 14b shows the effect of the tilt angle on the  $F_z$  at the three spindle speeds. The observed trend is that, increase in the tilt angle decreases the value of  $F_z$  at all speeds. Also for a given tilt angle, increase in the spindle speed caused an increase in the  $F_z$ . In Fig. 14c, the variation of  $F_z$  with respect to tilt angle at different tool diameters was shown. It can be observed that, at a given tool pin diameter, an increase in the tilt angle caused a reduction in the value of  $F_z$ , while for any tilt angle, increase in the tool diameter caused an increase in the  $F_z$ .

### 5.6 Effect of process parameters on UTS

Interaction effect of the process parameters is shown in Fig. 15. Change in the UTS for different tool pin diameters at 2000, 2500 and 3000 rpm of spindle speed is shown in Fig. 15a. It was observed that there is a reduction of UTS for the three diameters from 2000 to 3000 rpm of spindle

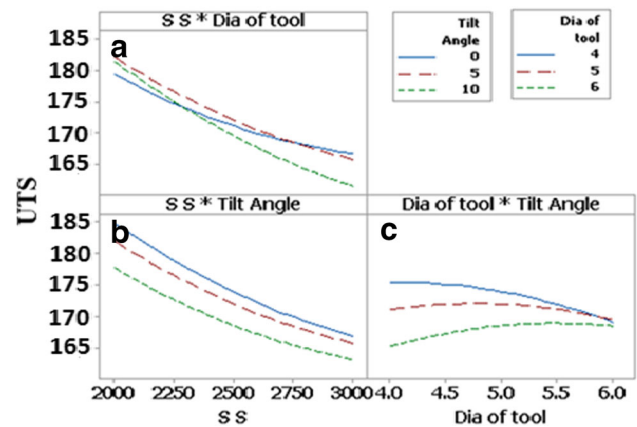


Fig. 15 Interaction effect of parameters on UTS

speeds. But the reduction in UTS at 4 mm tool pin diameter was found to be relatively low.

Interaction effect of spindle speed and tilt angle is shown in Fig. 15b. There was reduction in the UTS from 2000 to 3000 rpm of spindle speeds for the three tilt angles. But the UTS values were found to be more for 0° tilt angle than the 5° and 15° at the three spindle speeds.

Variation in the UTS for three tilt angles at different tool pin diameters is shown in Fig. 15c. It was found that the UTS increases for the tilt angle 10° from 4 to 6 mm tool pin diameter and the UTS decreases from 4 to 6 mm tool pin diameter for the tilt angle 0°. There was mixed effect on the UTS for the tilt angle 5°, but the change in the UTS is not much significant. UTS values for three tilt angles were found to be close for 6 mm diameter of tool pin.

## 6 Conclusions

The present study deals with experimental and numerical simulation investigation on shear flow of metal, tool vibration, welding forces in X, Y and Z directions and ultimate tensile strength in FSW of an aluminium 6061 alloy. Effect of spindle speed, tool pin diameter and tilt angle was also studied. The following highlights were drawn from this work:

- It was observed that the size of shear zone is mainly affected by tool rotational speed and diameters of pin. The tilt angle has very less effect.
- Spindle speed, tool pin diameter and interaction of spindle speed with tilt angle and tool pin diameter have significant effect on the amplitude of tool vibration.
- Spindle speed and tilt angle have significant effect on the ultimate tensile strength. Among the three parameters, tool pin diameter and tilt angle have significant effect on the  $F_x$  and  $F_z$ , respectively.

- Spindle speed and interaction of spindle speed and tool pin diameter have significant effect on the  $F_y$ .
- Amplitude of tool vibration, welding forces were predicted with FEM simulation and compared with experimental results. FEM simulation can be used to understand mechanics of friction stir welding.

**Acknowledgements** This work (Major project) was funded by Science and Engineering Research Board, Department of Science and Technology, Government of India. Grant no.: SERB/F/1761/2015-16.

## References

1. Thomas MW, Nicholas ED, Needham JC (1993) Improvements relating to friction welding international patent application no. PCT/GB92/02203, UK
2. Flores OV, Kennedy C, Murr LE (1998) Micro structural issues in a friction stir welded aluminium alloy. *Scr Mater* 38(5):703–708
3. Ghaffarpour M, Aziz A, Hejazi T-H (2015) Optimization of friction stir welding parameters using multiple response surface methodology. *Proc I Mech E Part L J Mater Design Appl*. <https://doi.org/10.1177/1464420715602139>
4. Arora KS, Pandey S, Schaper M, Kumar R (2010) Effect of process parameters on friction stir welding of aluminum alloy 2219-T87. *Int J Adv Manuf Technol* 50:941–952
5. Gadakh Vijay S, Kumar Adepu (2014) Friction stir welding window for AA6061-T6 aluminium alloy. *Proc I Mech E Part B J Eng Manuf* 228(9):1172–1181
6. Buchibabu V, Reddy GM, Kulkarni D, De A (2016) Friction stir welding of a thick Al–Zn–Mg alloy plate. *J Mater Eng Perform* 25:1163–1171
7. Sorensen CD, Stahl AL (2007) Experimental measurements of load distributions on friction stir weld pin tools. *Metall Mater Trans B* 38:451–459
8. Kasman Sxefika, Kahraman Fatih (2014) Investigations for the effect of parameters on the weld performance of AA 5083-H111 joined by friction stir welding. *Proc I Mech E Part B J Eng Manuf* 228(8):937–946
9. Balaji Srinivasan, Mahapatra Manas M (2012) Experimental study and modeling of friction stir welding process to produce optimized AA2219 butt welds for aerospace application. *Proc I Mech E Part B J Eng Manuf* 227(1):132–143
10. Neto DM, Neto P (2013) Numerical modeling of friction stir welding process: a literature review. *Int J Adv. Manuf Technol* 65:115–126
11. Das Bipul, Pal Sukhomay, Bag Swarup (2017) Design and development of force and torque measurement setup for real time monitoring of friction stir welding process. *Measurement* 103:186–198
12. Zhong YB, Wu CS, Padhy GK (2017) Effect of ultrasonic vibration on welding load, temperature and material flow in friction stir weldin. *J Mater Process Technol* 239:273–283
13. Pashazadeh Hamed, Masoumi Abolfazl, Teimournezhad Jamal (2013) A study on material flow pattern in friction stir welding using finite element method. *Proc I Mech E Part B J Eng Manuf* 227(10):1453–1466
14. Shojaeefard Mohammad Hasan, Khalkhali Abolfazl, Akbari Mostafa, Asadi Parviz (2015) Investigation of friction stir welding tool parameters using FEM and neural network. *Proc I Mech E Part L J Mater Design Appl* 229(3):209–217
15. Trimble D, Monaghan J, O'donnell GE (2012) Force generation during friction stir welding of AA2024-T3. *CIRP Ann Manuf Technol* 61:9–12
16. Kumar Sanjay, Kumar Sudhir (2015) Multi-response optimization of process parameters for friction stir welding of joining dissimilar Al alloys by gray relation analysis and Taguchi method. *J Braz Soc Mech Sci Eng* 37:665–674
17. Papahn Hossein, Haghpanahi Mohammad, Bahemmat Pouya (2017) Using a novel fixture to study of temperature and applied forces during friction stir welding. *J Braz Soc Mech Sci Eng* 39:531–541
18. Sato YS, Urata M, Kokawa H (2002) Parameters controlling microstructure and hardness during friction stir welding of precipitation-hardenable aluminum alloy 6063. *Metall Mater Trans A* 33A–3:625–635
19. Su H, Wu CS, Pittner A, Rethmeier M (2013) Simultaneous measurement of tool torque, traverse force and axial force in friction stir welding. *J Manuf Process* 15:495–500
20. Shi L, Wu CS (2017) Transient model of heat transfer and material flow at different stages of friction stir welding process. *J Manuf Process* 28:323–339
21. Dialami N, Chiumenti M, Cervera M, Segatori A, Osikowicz W (2017) Enhanced friction model for friction stir welding (FSW) analysis: simulation and experimental validation. *Int J Mech Sci* 133:555–567
22. Mostafapour Amir, Ebrahimpour Ali, Saeid Tohid (2017) Numerical and experimental study on the effects of welding environment and input heat on properties of FSSWed TRIP steel. *Int J Adv Manuf Technol* 90:1131–1143
23. Pei Xianjun, Dong Pingsha (2017) A selectively-coupled shear localization model for friction stir welding process window estimation. *Int J Mach Tools Manuf* 123:89–104
24. Dialami N, Cervera M, Chiumenti M, Agelet de Saracibar C (2017) Local–global strategy for the prediction of residual stresses in FSW processes. *Int J Adv Manuf Technol* 88:3099–3111
25. Raghulapadu JK, Peddieson J, Buchanan GR (2008) A rotating plug model of friction stir welding heat transfer. *Heat Transf Eng* 29(3):321–327
26. Mahoney MW, Rhodes CG, Flintoff JG (1998) Properties of friction-stir-welded 7075 T651 aluminum. *Metall Mater Trans A* 29:1955–1964